METHODS PAPER



An Adaptive SCG-ECG Multimodal Gating Framework for Cardiac CTA

Shambavi Ganesh¹ • Mostafa Abozeed² • Usman Aziz² • Srini Tridandapani² • Pamela T. Bhatti¹

Received: 10 March 2024 / Revised: 18 September 2024 / Accepted: 30 September 2024 © The Author(s) under exclusive licence to Society for Imaging Informatics in Medicine 2024

Abstract

Cardiovascular disease (CVD) is the leading cause of death worldwide. Coronary artery disease (CAD), a prevalent form of CVD, is typically assessed using catheter coronary angiography (CCA), an invasive, costly procedure with associated risks. While cardiac computed tomography angiography (CTA) presents a less invasive alternative, it suffers from limited temporal resolution, often resulting in motion artifacts that degrade diagnostic quality. Traditional ECG-based gating methods for CTA inadequately capture cardiac mechanical motion. To address this, we propose a novel multimodal approach that enhances CTA imaging by predicting cardiac quiescent periods using seismocardiogram (SCG) and ECG data, integrated through a weighted fusion (WF) approach and artificial neural networks (ANNs). We developed a regression-based ANN framework (r-ANN WF) designed to improve prediction accuracy and reduce computational complexity, which was compared with a classification-based framework (c-ANN WF), ECG gating, and US data. Our results demonstrate that the r-ANN WF approach improved overall diastolic and systolic cardiac quiescence prediction accuracy by 52.6% compared to ECG-based predictions, using ultrasound (US) as the ground truth, with an average prediction time of 4.83 ms. Comparative evaluations based on reconstructed CTA images show that both r-ANN WF and c-ANN WF offer diagnostic quality comparable to US-based gating, underscoring their clinical potential. Additionally, the lower computational complexity of r-ANN WF makes it suitable for real-time applications. This approach could enhance CTA's diagnostic quality, offering a more accurate and efficient method for CVD diagnosis and management.

 $\textbf{Keywords} \ \ \text{Cardiovascular disease} \cdot \text{Cardiac computed tomography angiography (CTA)} \cdot \text{Seismocardiography (SCG)} \cdot \text{Electrocardiography (ECG)} \cdot \text{Ultrasound (US)} \cdot \text{Artificial neural network (ANN)}$

Introduction

Cardiovascular disease (CVD) results in the loss of more than 17.9 million lives annually, as reported by the World Health Organization (WHO) [1]. CVDs are disorders of the heart and blood vessels that affect people of all ages, ethnicities, and backgrounds. In the United States alone, approximately 18.2 million people suffer from coronary artery disease (CAD), the most common type of CVD, contributing to more than 610,000 deaths annually [2]. The current gold standard for the assessment of coronary blood vessel blockage is catheter coronary angiography (CCA), a procedure

that involves the insertion of catheters into coronary vessels [3]. While CCA provides high-resolution images of coronary vessels, its invasive nature [4] and associated costs [5] present non-trivial risks for the patients.

Cardiac computed tomography angiography (CTA), an alternative to CCA for CVD evaluation, utilizes a computed tomography (CT) scanner and intravenous contrast agent to produce high-resolution, three-dimensional representations of coronary vessels. CTA offers several advantages, including reduced invasiveness, leading to fewer complications, quicker procedures, and lower costs, while potentially achieving diagnostic image quality like that of CCA [6, 7]. As a result, CTA serves as an effective diagnostic tool that is particularly suitable for individuals with low to intermediate CVD risk. However, CTA suffers from limited temporal resolution, which affects the diagnostic quality of reconstructed images due to motion artifacts. This hinders the widespread adoption of CTA as the mainstream diagnostic tool for CVD

Published online: 15 October 2024



Shambavi Ganesh shambavi.ganesh@gatech.edu

Department of Electrical and Computer Engineering, Georgia Institute of Technology, Atlanta, GA, USA

Department of Radiology, University of Alabama at Birmingham, Birmingham, AL, USA

Fig. 1 A labeled ECG waveform. Salient ECG features such as the P wave, QRS complex, T-wave, systole, and diastole are depicted. The systolic and diastolic QPs are highlighted along with the duration from the R-peak to the QP centers, Δt^s_{ecg} and Δt^d_{ecg} , respectively

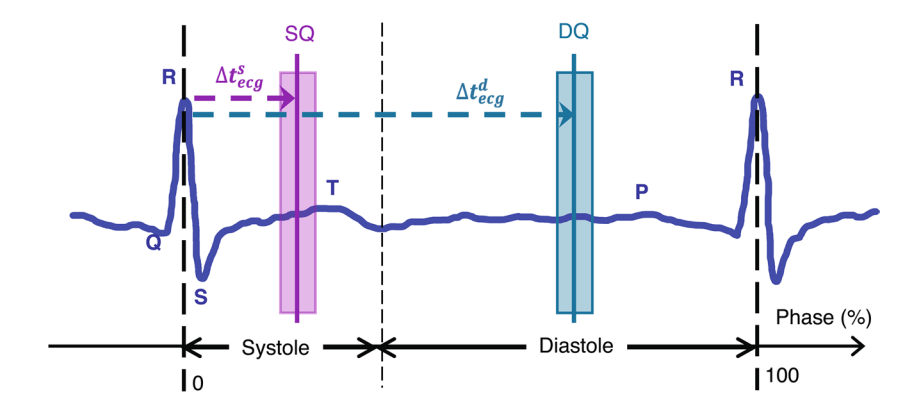


Table 1 Summary of key ECG salient features

ECG terms	Description
R, Q, S, T, P	ECG waveform components representing electrical activity
Δt^{s}_{ecg}	Interval between R wave and onset of systolic quiescence
$\Delta t^{s}_{ m ecg} \ \Delta t^{d}_{ m ecg}$	Interval between R wave and onset of diastolic quiescence
Systole	Contraction phase of the heart (R wave to end of T wave)
Systolic quiescence (SQ)	Period during systole when the heart exhibits minimal motion
Diastole	Relaxation phase of the heart (after T wave until next R wave)
Diastolic quiescence (DQ)	Period during diastole when the heart shows minimal motion

evaluation, making it imperative to increase the accuracy of cardiac quiescent period prediction during CTA acquisition.

Accurate detection of cardiac quiescence is essential for CVD diagnosis, as it directly improves the quality of imaging techniques like cardiac CTA. By precisely identifying the heart's quiescent phases, during which it remains relatively motionless, clearer and more accurate diagnostic images can be obtained. This enhancement in image quality significantly increases the reliability of CVD diagnosis and leads to better patient outcomes. Therefore, the ability to predict cardiac quiescence represents a significant advancement in cardiovascular diagnostics.

Presently, real-time electrocardiography (ECG) is routinely used for CTA gating due to readily identifiable ECG features, such as the QRS complex and R-peaks [8] as shown in Fig. 1. The salient characteristics are summarized in Table 1. While ECG effectively measures cardiac electrical activity, it does not adequately capture the inherent mechanical motion of the heart, rendering it suboptimal as a triggering mechanism for CTA. Moreover, the considerable variety of ECG gating functions found in the literature underscores a lack of conformity and standardization in this approach [9–11]. These limitations have spurred investigations into other modalities, such as seismocardiography (SCG) [12] and ultrasound (US) [13].

Previous studies have explored the potential of SCG as a predictor of cardiac quiescence. SCG records cardiac mechanical vibrations through the placement of an accelerometer on the chest wall and accurately depicts

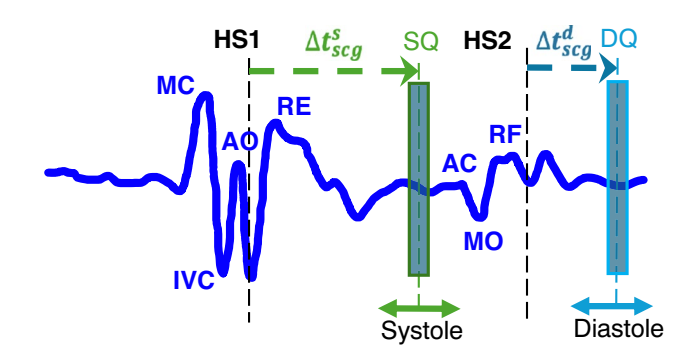


Fig. 2 A labeled SCG waveform. Salient SCG features such as heart sounds (HS1 and HS2), mitral valve closing (MC), aortic valve opening (AO), rapid ejection (RE), aortic valve closing (AC), mitral valve opening (MO), and rapid filling (RF) are depicted. The systolic and diastolic QPs are highlighted along with Δt^s_{scg} and Δt^d_{scg}

the mechanical state of the heart [14]. Key characteristics of an SCG signal are illustrated in Fig. 2 and further elaborated in Table 2. An SCG patient-specific template approach combined with heart rate prediction was utilized to identify and detect cardiac quiescence [15]. The SCG-based gating strategy demonstrated greater accuracy in predicting systolic and diastolic quiescent periods than traditional ECG-based gating. While SCG-based cardiac gating is promising, several limitations must be addressed to standardize its use. One major limitation is the susceptibility of SCG signal quality to noise, primarily due to the high sensitivity of accelerometers to motion artifacts



Table 2 Summary of key SCG salient features

SCG terms	Description		
MC (mitral closure)	Mitral valve closure; onset of systole		
AO (aortic opening)	Aortic valve opens; blood ejected from left ventricle		
RE (rapid ejection)	Rapid ejection of blood into aorta and pulmonary artery		
Systole	Cardiac cycle phase wherein the heart muscles contract, pumping blood out of the chambers		
Systolic quiescence (SQ)	Period of minimal motion during systole		
AC (aortic closure)	Aortic valve closure; end of systole		
MO (mitral opening)	Mitral valve opens; onset of diastole		
RF (rapid filling)	Rapid filling of ventricles from atria		
Diastole	Cardiac cycle phase wherein the heart muscles relax, allowing the chambers to fill with blood		
Diastolic quiescence (DQ)	Period of minimal motion during diastole		
HS1 (first heart sound)	Closure of mitral and tricuspid valves		
HS2 (second heart sound)	Closure of aortic and pulmonary valves		
$\Delta t^{ m d}_{ m scg}$	Interval between HS2 and onset of diastolic quiescence		
Δt^{s}_{scg}	Interval between HS1 and onset of systolic quiescence		

[16]. Additionally, even in patient-specific approaches, failure to detect SCG waveforms may occur due to distortion of heart sound peaks, stemming from physiological variability, leading to incorrect cardiac quiescence predictions [17, 18].

While SCG effectively measures the true mechanical state of the heart and is cost-effective, waveform inconsistency prevented its adoption over traditional ECG-based cardiac QP prediction. Additionally, at higher heart rates, ECG-based quiescence predictions were more accurate as compared to SCG [19]. Combining SCG and ECG could enhance cardiac quiescence prediction by leveraging the strengths of both modalities. This integrated approach aims to overcome the limitations of each individual modality, potentially leading to more accurate and reliable cardiac assessments.

These findings provide an empirical foundation for multimodal cardiac quiescence prediction frameworks. This paper builds upon earlier work involving a SCG-based quiescence prediction method and a weighted fusion (WF), SCG-ECG-based classification artificial neural network (ANN) framework (c-ANN WF) [20]. Building upon this work, a modification of the previously utilized weighted fusion framework is implemented using a regression approach, henceforth referred to as the r-ANN WF. The primary aim of this study is to determine whether the r-ANN WF can achieve comparable or improved prediction accuracy relative to the c-ANN WF while offering reduced computational time enabling real-time clinical applications. Additionally, a blinded observer study validates the results by comparing the accuracy of the r-ANN framework with c-ANN, ECG, and US prediction frameworks.

Methods

Subjects and Data Acquisition

We collected trimodal cardiac data, including ECG, SCG, and US measurements, from two groups: 11 healthy subjects (mean age: 26; age range: 22-48; female/male ratio: 4/7) and 17 subjects with cardiac abnormalities (mean age: 62; age range: 31-80; female/male ratio: 8/10). The Emory University Institutional Review Board approved the data collection, and each patient provided full written informed consent [17, 20]. The first subset of data includes synchronous ECG and SCG signals (Figs. 1 and 2), along with simultaneously acquired US and ECG signals. These data were collected using a custom trimodal system [20] in conjunction with a commercial ultrasound machine, the SonixTOUCH Research Scanner (Analogic, Peabody, MA, USA). Additionally, a set of cardiac signal data was collected using a modified data acquisition approach, wherein a BIOPAC MP150 (BIOPAC Systems Inc., Goleta, CA, USA) system simultaneously acquired SCG-ECG signals [17]. During the data acquisition process, synchronous SCG-ECG signals were recorded in 10-s bursts at a rate of 1.2 kHz during subject breath-hold. B-mode US data of the apical four-chamber view of the heart were acquired at a rate of 50 Hz using the commercial ultrasound machine. Simultaneously, another set of ECG data was collected at a rate of 200 Hz. These two sets of ECG data helped synchronize and align the US and SCG data.

For the acquisition and reconstruction of retrospective CTA data, two CT scanners were used, namely, the Siemens Somatom Definition dual-source 64-slice CT scanner and the Siemens Force dual-source 192-slice CT scanner



(Siemens Corp., Erlangen, Germany). Subsequently, two radiologists evaluated the diagnostic quality of the reconstructed CTA data for 17 patients with underlying cardiac defects in a blinded observer study.

Preprocessing Data

The preprocessing steps closely follow those described in previous work [19]. To address issues such as baseline drift and high-frequency noise, commonly present in raw ECG and SCG signals, we applied a 256th-order finite impulse response (FIR) low-pass filter. This filter, configured with a Hamming window and a cutoff frequency of 50 Hz, effectively conditioned both ECG and SCG signals, preserving the QRS complex in the ECG signal and the high-frequency heart sounds (HS1 and HS2) in the SCG signal. Next, we utilized a notch filter with a center frequency of 0 Hz and a bandwidth of 1 Hz to eliminate DC signals, thereby removing any remaining baseline drift [19]. To empirically evaluate the necessity of these steps, we conducted a comparative analysis using two models: r-ANN WF and c-ANN WF. The models were trained and tested both with and without the preprocessing steps, and their performances were compared. The B-mode US images underwent Gaussian noise removal and contrast enhancement. Additionally, the acquired and preprocessed signals were synchronized with one another, ensuring their alignment and coherence for subsequent analysis and interpretation.

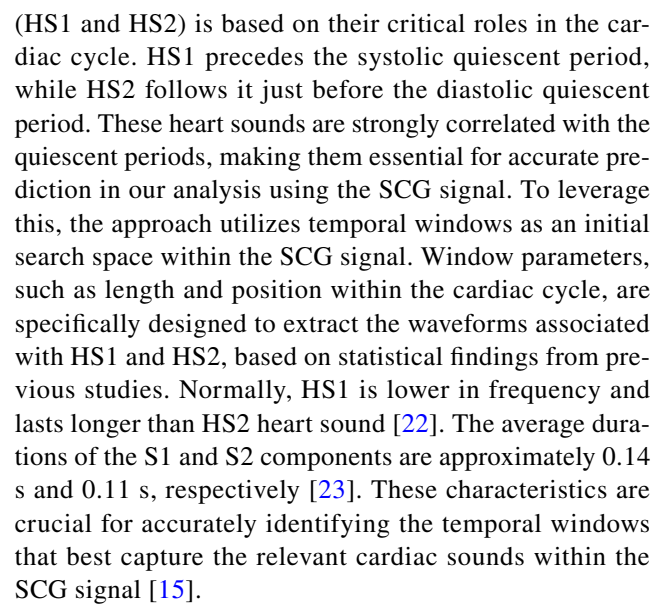
US-Based Cardiac Quiescence Baseline

The baseline for quiescence is defined as the minimum magnitude of the velocity vector corresponding to the interventricular septum (IVS) in the B-mode US data. This magnitude is computed using the phase-to-phase deviation measure [21]. To enhance the reliability of the identified quiescent periods, we implement a patient-specific voting mechanism. Previously described in analogous research, this mechanism contributes to the robustness and accuracy of quiescence period determination within our study framework [15].

SCG-Based and ECG-Based Quiescence Prediction

SCG-Based Quiescence Prediction

An overview of previously demonstrated methods used for the detection and prediction of cardiac quiescence using SCG signals [15, 19] is presented. SCG signals contain significant heart sound features which are closely associated with systolic and diastolic quiescent periods, exhibiting temporal proximity distinct from that of the ECG signal. The selection of the first and second heart sounds



Next, two heart sound-associated waveforms are generated through the application of the Hilbert transform [24] to capture the temporal characteristics and high-frequency components present in the SCG signal. Then, a heart ratebased phase delay function is computed to characterize the relationship between the delay observed between the peaks in the heart sound-based waveforms and the USbased quiescent periods. Notably, heart rate is predicted using a linear regression-based technique, given that the heart rate for upcoming cardiac cycles is unknown. Previous studies have demonstrated a linear relationship between quiescent phases (expressed as a percentage of the cardiac cycle) derived from both SCG and echocardiography, in relation to heart rate [25]. By establishing a relationship between cardiac quiescence (in percentage phase) and heart rate (bpm), the timing of quiescent phases across varying heart rates is predicted, which is crucial for optimizing image acquisition during quiescent periods. This approach facilitates the prediction of quiescent periods, denoted as P_{scg} , during patient-specific SCG-based cardiac gating.

ECG-Based Quiescence Prediction

Currently, real-time ECG constitutes the gold standard during prospective CTA gating, predominantly due to identifiable ECG features such as the QRS complex and R peaks. For ECG-based cardiac gating, the piecewise function of the Siemens Force scanner was used based on salient features to generate ECG-based results for this fusion gating framework [17, 26]. The interval from the R-peak to the start of the QP, shown in Fig. 1, is predicted every cardiac cycle. The quiescence prediction derived from the CTA ECG gating function is denoted by P_{ecg} .



r-ANN Prediction Framework

The fusion r-ANN prediction framework utilizes probability coefficients, w_{ecg} and w_{scg} , as weights to optimally combine predictions from both ECG (P_{ecg}) and SCG (P_{ecg}) signals, respectively. These probability weights are critical because they represent the relative confidence of each signal's prediction. By incorporating these estimates, the model dynamically adjusts the influence of each signal in the final prediction, improving accuracy. While the ECG-SCG module does not directly output predictions, it provides key features for the ANN to generate these probability values. This approach ensures that the final quiescent period prediction is a weighted average, maximizing accuracy by leveraging both signals.

Feature Extraction and Selection

Patient-specific features were extracted from the preprocessed ECG and SCG signals after normalizing cardiac cycle lengths. Previous research has shown the effectiveness of a comprehensive feature set, including heart rate (HR), heart rate variability (HRV), wavelet-based features, signal-to-noise ratio, and power spectrum coefficients, for cardiac quiescence prediction [19]. To reduce computational complexity for real-time processing, recent studies identified a revised feature set [27]. This selection process pinpointed specific features that enhance predictive accuracy, as outlined in Table 3.

Initially, a feature set consisting of ten features was derived from the ECG and SCG signals. The ECG features include HR, HRV, signal-to-noise ratio, discrete wavelet transform (DWT) coefficients, and autoregressive coefficients (AR₅(7) and AR₆(7)) [28]. The SCG features include power spectral density of HS1 and HS2, short-term Fourier transform (STFT) coefficients [29], and DWT coefficients [30]. Principal component analysis (PCA) was applied to this feature set to evaluate the contribution of each feature to the overall model accuracy [31]. Based on the outcomes of this analysis, four final features were selected—two from

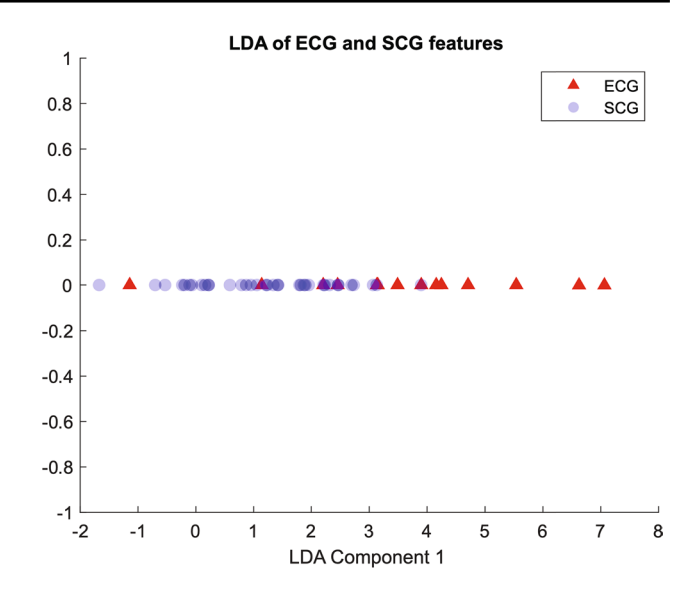


Fig. 3 Linear discriminant analysis (LDA) of features: the plot illustrates the separation between two classes based on the first LDA component derived from four features. The classes are represented by different markers and colors (ECG: red triangles, SCG: blue circles). Despite the original four-dimensional feature space, the LDA reduction shows how the features contribute to distinguishing between the two classes in a one-dimensional space

the ECG signal and two from the SCG signal. The selected features for the ECG signal were $AR_5(7)$ and $AR_6(7)$, and for the SCG signal, they were the variance from the STFT coefficients and the mean of the DWT coefficients. Only eigenvalues accounting for less than 20% of the largest eigenvalues were discarded. Additional figures pertaining to the features are included (Online Resource 1).

Next, linear discriminant analysis (LDA) was applied to assess the ability of the extracted features to differentiate between SCG-based and ECG-based QP predictions [32]. LDA maximizes the ratio of between-class to withinclass variance, ensuring optimal separability. Four features were used as input, and since the data has two classes, LDA reduced the feature space to a single dimension (LDA component 1), as shown in Fig. 3. The resulting scatter plot

Table 3 Details of the extracted features from the ECG and SCG signals

Feature set	Originated signal	Computed features	Number of features extracted	Extracted features	References
Autoregressive model (AR _{ecg})	ECG	Coefficients of AR model	2	5th and 6th coefficients of order 7 AR model	[28]
Short-time Fourier transform (STFT _{scg})	SCG	Mean and variance of frequency spectrum	1	Variance of STFT coefficients	[29]
Discrete wavelet transform (DWT_{scg})	SCG	Mean and variance of coeffi- cients generated using Coif5 mother wavelet	1	Mean of DWT coefficients	[30]



shows some degree of class separation, but the overall data distribution suggests a non-linear nature to the problem. This finding supports the use of neural networks, which are well-suited to model complex, non-linear relationships by leveraging hypersurfaces in the feature space. Despite the original four-dimensional complexity, LDA's reduction to one dimension still preserves meaningful class separability, validating the robustness of the chosen features. These features were subsequently used as input into the ANN for further analysis. The features successfully demonstrated the most significant impact on predicting accuracy, thereby reducing the dimensionality of the input space while retaining critical information for the model.

Training and Testing

This study involved two distinct subject cohorts: 11 healthy individuals and 17 with cardiac conditions, as detailed in the acquisition section. The data is partitioned into training, validation, and testing sets, utilizing a leave-one-out method within each cohort, with a 4:1 ratio for testing and

Table 4 Summary of ANN architecture details

Component	Details
Number of input features	4 (selected from ECG and SCG signals)
Number of output neurons	2 (weights for ECG and SCG predictions)
Size of training set	Average of 5271 cardiac cycles per subject
Size of test set	Average of 1368 cardiac cycles per subject
Training data selection	Subset of size four times the testing dataset, selected blindly to avoid over-training

training data. The model is trained on data from the subject cohort, excluding the data from the subject under evaluation. A fourfold cross-validation approach is used within each cohort, repeated 10 times for the validation dataset. Table 4 provides details on training/testing conditions and the ANN architecture.

Artificial Neural Network Configuration

An overview of generating an SCG-ECG derived fusion QP is detailed in Fig. 4. The pipeline starts by extracting features from ECG and SCG signals, which are then fed into an artificial neural network (ANN) module. Next, prediction weights for both signals, w_{ecg} and w_{scg} , derived from the ANN module are subsequently combined with the ECG and SCG quiescent period predictions, P_{ecg} and P_{scg} . The r-ANN fusion framework utilized in this research is structured with an input layer, 2 hidden layers, and an output layer. Specifically, the ANN configuration in this study is a three-layer feed-forward network. The input to the ANN consists of a set of four features extracted from both the ECG and SCG signals. The ANN produces outputs in the form of probability coefficients, which in turn provide weights for the fusion of ECG and SCG predictions, detailed in Fig. 5 and summarized in Table 5. The following Eq. (1) is utilized to combine the r-ANN derived weights and SCG-ECG QP predictions, to generate the final weighted fusion QP, F_{QP} :

$$F_{QP} = P_{scg} * w_{scg} + P_{ecg} * w_{ecg}$$
 (1)

The hidden layers utilize hyperbolic tangent-sigmoid and log-sigmoid activation functions, while the outer layer utilizes the softmax activation function. The tansig activation function is mathematically represented as:

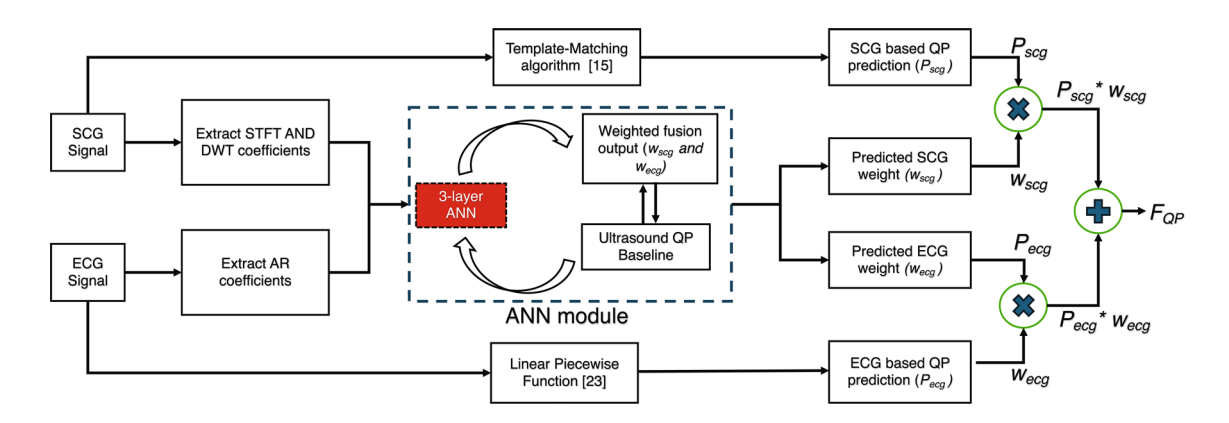


Fig. 4 ANN-based cardiac gating framework. In the upper branch, STFT and DWT coefficients are extracted from the preprocessed SCG signals. In the lower branch, AR coefficients are extracted from preprocessed ECG signals. Next, the features are input into the ANN

module to generate w_{ecg} and w_{scg} , which is then combined with P_{ecg} and P_{scg} , respectively, leading to the computation of the fusion prediction value, F_{OP}



Fig. 5 Architecture of the regression-based artificial neural network (r-ANN WF) used in the study. The network consists of an input layer with 4 features, two hidden layers with 3 neurons each, and an output layer with 2 neurons. The output neurons provide the probability weights (w_{seg} and w_{eeg}) for the fusion of SCG and ECG predictions

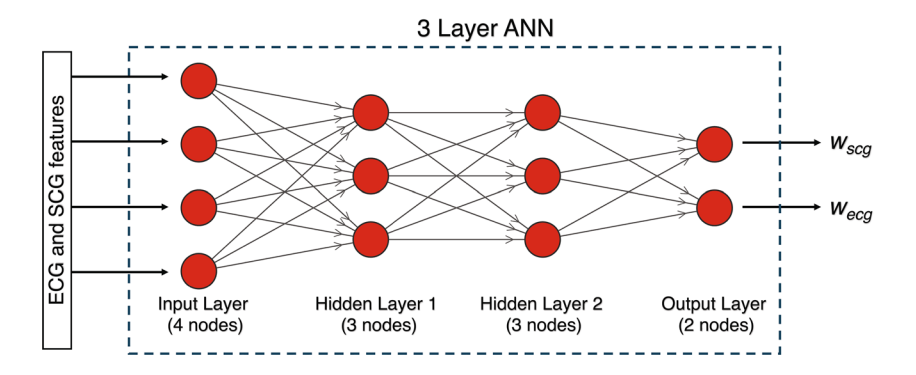


Table 5 Summary of ANN outputs and optimization details

Component	Description	Values/details
ANN outputs	Outputs used for the fusion of ECG and SCG predictions, interpreted as coefficients or scores	Two outputs (w_{ecg} and w_{scg})
Fusion function	Function that combines ECG and SCG predictions using the weights from the ANN outputs	Fusion prediction = $w_{ecg} * P_{ecg} + w_{scg} * P_{scg}$
Activation functions	Functions used in the hidden and output layers of the ANN	Hidden 1: tansig; hidden 2: logsig; output: softmax
Optimization	Method used to train the ANN and optimize the model's performance	Adam optimizer
Loss function	Function used to quantify the performance of the model during training	Cross-entropy loss function
Output units	The unit of the final outputs from the ANN module	Milliseconds

$$tansig(x) = \frac{2}{1 + e^{-2x}} - 1 \tag{2}$$

The log-sigmoid activation function is given by:

$$\log \operatorname{sig}(x) = \frac{1}{1 + e^{-x}} \tag{3}$$

The output layer uses the softmax activation function which converts the output logits into probability weights, ensuring that the sum of all probabilities equals 1, is given as follows:

$$\operatorname{softmax}(z_i) = \frac{e^{z_i}}{\sum_{j=1}^n e^{z_j}}$$
(4)

This architecture was trained using the Adam optimizer, which is widely recognized for its efficiency and robustness in model optimization [33]. Additionally, the cross-entropy loss function is utilized to quantify the model's performance.

The regression approach adopted in this study allows the ANN to predict continuous values, specifically the timing of quiescent periods in milliseconds, rather than discrete class labels. In this context, regression is coupled with the ANN by directly feeding the network with the US-derived quiescent periods as target values during training, as shown in Fig. 4. This approach differs from traditional classification tasks (c-ANN) where the output would be a categorical label, such as "systolic" or "diastolic." By using a regression

framework, the ANN learns to map input features (extracted from ECG and SCG signals) to a continuous output representing the exact timing of quiescent phases within the cardiac cycle. This eliminates the need for classification labels, as the focus shifts from predicting categorical outcomes to estimating precise temporal intervals, thereby enhancing the model's applicability in scenarios where exact timing is critical for minimizing motion artifacts in CTA imaging.

Results

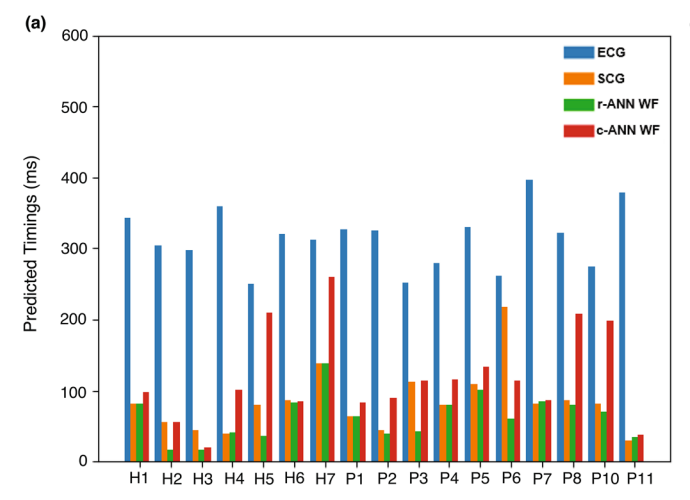
The efficacy of the r-ANN multimodal framework is measured through performance metrics including the quantification of errors associated with quiescence predictions generated by artificial neural networks (ANNs) and the comparison of computational time to prior work. The following subsections detail the prediction results, computational times, and comparison of CTA grades.

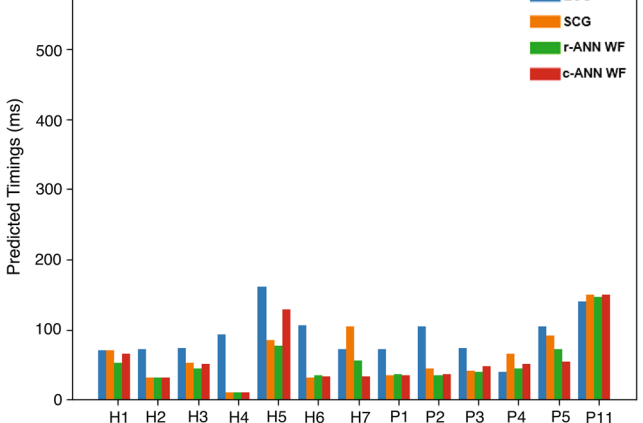
Quiescence Prediction Accuracy

The quiescence prediction accuracy is primarily dependent on the prediction error (in milliseconds), defined as the absolute difference between the predicted quiescent timing and that of the subject-specific US-derived ground truth. The degree of degradation of the reconstructed CTA images is



ECG





600

Fig. 6 Comparison of predicted quiescence error timings across multiple frameworks. a Prediction error timings (in milliseconds) are compared across a subset of patients based on diastole prediction

values. This is done across ECG, SCG, r-ANN, and c-ANN. **b** Systole prediction error timings (in milliseconds) across the ECG, SCG, r-ANN, and c-ANN

sensitive to mistiming during the predicted quiescent periods. The prediction errors of the regression-based ANN framework (r-ANN WF) are compared to those of the prediction times from the ECG gating framework, SCG gating framework, and previously established classification-based ANN framework (c-ANN WF). Figure 6 compares the average prediction error (in milliseconds) for all cardiac cycles for diastole- and systole-based QPs for a subset of patients. Comparisons were conducted across various computational frameworks, including ECG, SCG, r-ANN WF, and c-ANN WF. Table 6 in the supplementary material (Online Resource 1) contains the comparison of diastolic and systolic error timings across all healthy and cardiac patients. On average, the r-ANN WF prediction framework improved overall diastolic and systolic cardiac quiescence prediction by 52.6% compared with ECG-based predictions when both are compared against the quiescence baseline, B-mode echocardiography.

Table 6 Comparison of computational times for prediction of quiescent periods between c-ANN WF and r-ANN WF frameworks, across varying number of cardiac cycles as input implemented using C++ and MATLAB

Number of cardiac cycles	C++implementation		MATLAB	
	c-ANN WF (millisec- onds)	r-ANN WF (millisec- onds)	c-ANN WF (millisec- onds)	r-ANN WF (millisec- onds)
1	5.61	4.83	26.55	21.72
10	5.65	4.90	27.83	22.36
100	7.21	5.48	30.42	25.59
1000	8.64	6.25	30.87	26.81
10,000	11.83	10.14	34.29	28.08
100,000	37.27	32.93	107.49	99.01

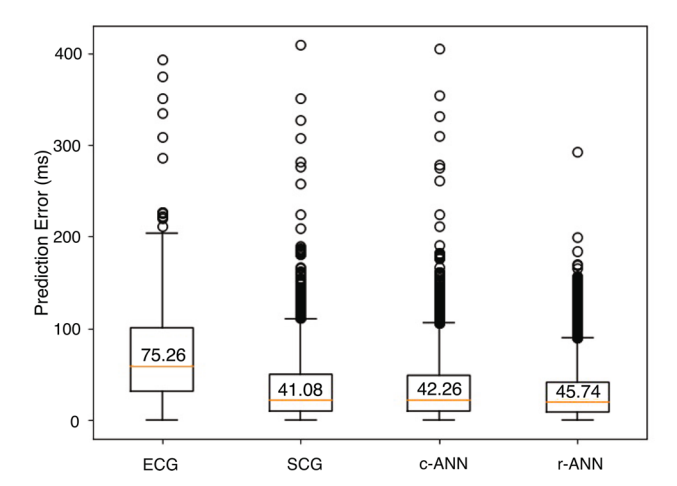


Fig. 7 Cumulative quiescence prediction errors (in milliseconds) for all subjects, depicted in a box plot. Median values (highlighted in yellow) with interquartile ranges are shown. ECG-based predictions exhibited the highest error, while SCG-based predictions, c-ANN WF, and r-ANN WF display comparable error rates. The r-ANN WF demonstrates less variability and median prediction error values as compared to c-ANN WF framework

There was an improvement of 7.8% in QP accuracy when comparing the r-ANN WF to the c-ANN WF. The cumulative prediction errors across all patients per framework are ECG-based (75.26 ms), SCG-based (41.08 ms), c-ANN WF (45.74 ms), and r-ANN WF (42.26 ms), as depicted in Fig. 7.

Computational Time

The computational complexity of the r-ANN WF is compared with that of the c-ANN WF. The number of input features (N) during both the forward and backward passes of



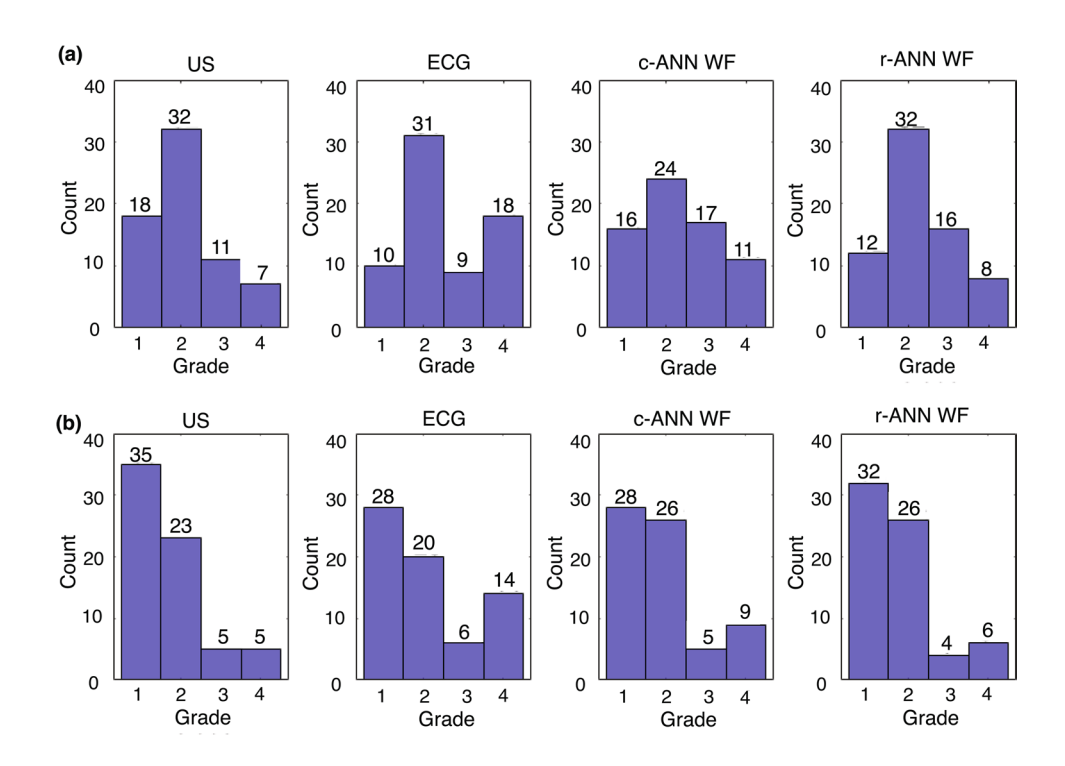
ANN prediction is a primary factor of determination, where the complexity is O(N). It should be noted that this does not include latency associated with feature extraction-based functions. The computational times for a QP prediction for a cardiac cycle, averaged across all patients, are 5.61 ms and 4.83 ms for the c-ANN WF and the r-ANN WF, respectively, when implemented using C + +. Additionally, when the algorithms were implemented in MATLAB (MATLAB version 9.13.0 (R2022b), Natick, MA, MathWorks, Inc.), the computational times were 26.55 ms for the c-ANN WF and 21.72 ms for the r-ANN WF. While these gains are modest, they may be the difference between the feasibility of realtime implementation or lack thereof. The reduction in computational time with r-ANN WF across platforms supports the improvement of real-time prediction models. The experiments were conducted on an Intel (core i7 10th gen, Intel Corporation, Santa Clara, CA, USA) laptop with an Nvidia graphics card (Nvidia Corporation, Santa Clara, CA, USA).

Comparison of CTA Grades

To assess the predictive accuracy of cardiac quiescence-based gating approaches, we reconstructed the CT volumes using phases derived from ECG, c-ANN WF, r-ANN WF, and baseline US quiescence predictions. These reconstructions were performed for a cohort of cardiac patients comprising 17 individuals. The diagnostic image quality of the left main (LM), left anterior descending (LAD), left circumflex (LCX), and right coronary arteries (RCA) was evaluated by two board-certified cardiothoracic

radiologists (hereafter referred to as observer 1 and observer 2) in a blinded observer study. The radiologists, with five (observer 1) and six (observer 2) years of subspecialized experience in cardiac imaging, respectively, were unaware of the source of the phase predictions. Ratings were assigned using a Likert response format where 1 = excellent, 2 = good, 3 = adequate, and 4 = non-diagnostic. Tables 4 and 5 (Online Resource 1) provide a detailed breakdown of the individual diagnostic quality assessments made by the two observers. The average grades assigned by observer 1 for the US, ECG, c-ANN WF, and r-ANN WF were 2.1 (p = 0.0315), 2.5, 2.3 (p = 0.0802), and 2.2 (p = 0.041), respectively. Similarly, the average grades given by observer 2 for the US, ECG, c-ANN, and r-ANN were 1.7 (p = 0.0028), 2.1, 1.9 (p = 0.089), and 1.7 (p = 0.041), respectively. Significance testing was performed using the two-sided Wilcoxon signed-rank test with a significance level (α) of 0.05. Figure 8 presents a histogram illustrating the distribution of grades across the reconstructed volumes for each modality, recalling that a lower average Likert scale value corresponds to superior diagnostic quality. To assess the level of concordance between observer 1 and observer 2, the unweighted Cohen's kappa test was used, yielding a calculated value of 0.3208 (p < 0.05). This kappa value, as per the established criteria delineated by Landis and Koch [34], denotes a level of agreement deemed fair. This blinding process was critical to mitigating potential bias, as the radiologists did not know whether they were evaluating images derived from US, ECG, or SCG predicted phases. Their

Fig. 8 Categorical comparisons between observer 1 (a) and observer 2 (b) interpretations are depicted using histograms. Categories (US, ECG, c-ANN WF, and r-ANN WF) are assessed on a Likert scale (1 = excellent, 2 = good, 3 = adequate, 4 = non-diagnostic)





assessments were focused solely on the quality of the reconstructed images, providing an objective measure of the efficacy of the r-ANN prediction framework.

Discussion

This study explores the benefits of utilizing a regressionbased ANN for cardiac quiescence prediction to enhance CTA prospective gating, a key diagnostic tool for CVD evaluation. The analysis compares the r-ANN WF framework with ECG, SCG, and c-ANN WF methods, each offering distinct merits and limitations. Understanding their relative advantages is vital for optimizing the accuracy and efficiency of CTA gating procedures. Prior research has extensively validated echocardiography as a reliable predictive tool for assessing cardiac quiescence [21, 35]. However, during this study, US gating was not feasible due to the lack of CT-compatible US transducers. Commercial US transducers cause streak artifacts that compromise CT scan quality. Therefore, in this investigation, US-based data primarily serve as baseline measurements of cardiac quiescence and provide a comparative analysis against predictions derived from SCG and ECG signals.

Existing methods, such as retrospective and prospective ECG gating, often suffer from delays in data processing and lack the capability for real-time application. In contrast, the r-ANN WF model combined with real-time prediction can be utilized to generate predictions based on individual patient data. By combining SCG and ECG, the r-ANN WF model provides a more robust and comprehensive prediction, improving the accuracy of quiescent period detection compared to models relying solely on ECG or SCG.

The use of regression models allows r-ANN to directly predict the timing of quiescent phases in milliseconds, providing a precise estimate of the cardiac cycle's quiescent periods. This level of accuracy is crucial for reducing motion artifacts in CTA images. The results highlight the significant impact of preprocessing on model performance. Specifically, the removal of preprocessing steps led to a notable decrease in model accuracy. For instance, the accuracy improvement of the r-ANN WF model over ECG-based predictions reduced from 52.6 to 46.3% when compared to the c-ANN model. Additionally, while the performance gap between the r-ANN and c-ANN models remained approximately 7%, there was an average decrease of 8.6% in individual prediction accuracy without preprocessing. Therefore, careful consideration of preprocessing techniques is essential to improve diagnostic outcomes.

Accurate quiescent period predictions allow CTA systems to synchronize image capture with heart motion, minimizing artifacts and enhancing the diagnostic quality of coronary artery reconstructions. The r-ANN WF proved to be more

computationally efficient with an average prediction time of 4.83 ms, as compared to the c-ANN WF which has a prediction time of 5.61 ms when implemented using C++. Additionally, Table 6 contains the comparison of computational efficiency for c-ANN WF and r-ANN WF with an increase in the number of cardiac cycles, across C++—and MATLAB-based implementations.

The cardiac cycle numbers chosen for input are arbitrary, designed to reflect the range of prediction times expected during real-time data processing. This efficiency stems mainly from the direct prediction of quiescent timings, eliminating the need for additional classification steps. For clinical implementation in prospective cardiac CTA gating, the r-ANN WF's lower computational complexity makes it highly suitable for real-time processing.

Among the four quiescence prediction frameworks, the baseline US-based method consistently achieved the highest average diagnostic quality, while the ECG-based method consistently showed the lowest. The observer study suggests that the US gating model is promising for CTA gating. Both the r-ANN WF and c-ANN WF frameworks perform closer to the US-based framework and surpass the conventional ECG framework. Furthermore, the diagnostic grades from the observer study indicate that the r-ANN's performance is comparable to the c-ANN framework.

A limitation of the observer study is the small sample size of patients and limited patient demographics. This restricts the generalizability of our findings across broader populations. Future studies should include a larger and more diverse cohort to validate the robustness of the r-ANN WF model across different demographic groups and clinical settings. Additionally, while the r-ANN WF improves overall prediction accuracy within the weighted fusion framework, its performance for outlier cases remains an area of concern. Specifically, ECG- or SCG-based prediction methods have shown higher accuracy for certain patient profiles, suggesting that the r-ANN WF may need further optimization or hybridization with other models to handle these edge cases more effectively. Further investigation is warranted to explore how patient-specific factors such as age, gender, and comorbidities might influence the model's predictions. Incorporating these factors into the model or creating a stratified approach could improve the r-ANN WF's adaptability and accuracy.

This work emphasizes the significance of alternative cardiac CTA gating methodologies based on prediction accuracy and computational complexity. The modified SCG-ECG framework can potentially be utilized for cardiac quiescence prediction. This study also presents the potential integration of SCG into clinical practice as a more accurate alternative to ECG for predicting cardiac quiescence. In the future, SCG could be implemented through the placement of accelerometers on the chest, like EKG



leads. This innovation would enable real-time quiescence prediction to gate CT scanners, enhancing the quality of cardiac imaging and improving patient outcomes by reducing motion artifacts and increasing diagnostic precision. Furthermore, multimodal SCG-based frameworks have emerged as advantageous in scenarios where the utilization of an US-based gating framework faces feasibility challenges, such as incompatible CT transducers and the need for US or echocardiography technologists.

Conclusions

In summary, this study has investigated the feasibility of a regression-based multimodal framework that combines SCG and ECG data through ANNs for predicting cardiac quiescent periods. The introduction of r-ANN WF improved cardiac quiescence prediction accuracy in addition to computational efficiency when compared with c-ANN WF; furthermore, the decreased prediction time renders it suitable for real-time applications in cardiac CT gating. Comparable diagnostic accuracy in the observer study was also observed across the US and r-ANN WF-based CT reconstructions. As CVD remains a leading cause of death worldwide, the findings of this research could lead to a method that potentially improves patient care and clinical practice. Further investigations of this multimodal framework may result in the adoption of r-ANN WF as a feasible improvement over traditional ECG gating in cardiac CTA acquisition.

Supplementary Information The online version contains supplementary material available at https://doi.org/10.1007/s10278-024-01289-2.

Acknowledgements This research was supported by the National Science Foundation [Award Number: 2122299]. The authors would express their gratitude to Jingting Yao and Carson A. Wick for their insightful discussions and support through this work.

Author Contribution Pamela T. Bhatti, Shambavi Ganesh and Srini Tridandapani contributed to the study conceptualization, methodology, and design. Data analysis and the original draft preparation were performed by Shambavi Ganesh. The observer's study was performed by Mostafa Abozeed and Usman Aziz. The review and editing of the manuscript was performed by Pamela T. Bhatti, and Srini Tridandapani. The supervision, project administration, and funding acquisition were performed by Pamela T. Bhatti, and Srini Tridandapani. All the authors have read and agreed to the submitted version of the manuscript.

Funding This work was supported by the National Science Foundation [Award Number: 2122299] grant.

Declarations

Ethics Approval The patient data used in this research were obtained under the approval of the Emory University Institutional Review Board, and full written informed consent was obtained from each of the patients.

Consent to Participate Full written informed consent was obtained from each of the patients included in the study.

Competing Interests The authors declare no competing interests.

References

- World Health Organization cardiovascular disease statistics. Available: https://www.who.int/health-topics/cardiovascular-diseases#tab=tab_1. Accessed 10 January 2023.
- Brown JC, Gerhardt TE, Kwon E: Risk factors for coronary artery disease. StatPearls. Treasure Island (FL): StatPearls Publishing; 2023
- Bourassa MG: The history of cardiac catheterization. The Canadian Journal of Cardiology, vol. 21, no. 12, pp. 1011–1014, 2005.
- Tavakol M, Ashraf S, and Brener SJ: Risks and complications of coronary angiography: A comprehensive review. Global Journal of Health Science, vol. 4, no. 1, p. 65, 2012.
- 5. Ganz P, Amarenco P, Goldstein LB, Sillesen H, Bao W, Preston GM, Welch KMA: SPARCL Steering Committee. Association of osteopontin, neopterin, and myeloperoxidase with stroke risk in patients with prior stroke or transient ischemic attacks: Results of an analysis of 13 biomarkers from the Stroke Prevention by Aggressive Reduction in Cholesterol Levels trial. Stroke, vol. 48, no. 12, pp. 3223–3231, 2017.
- Schmermund A, Marwan M, Hausleiter J, Barth S, Bruder O, Kerber S, Korosoglou G, Leber A, Moshage W, Schröder S, Schneider S, Senges J, Achenbach S: Declining radiation dose of coronary computed tomography angiography: German cardiac CT registry experience 2009–2014. Clinical Research in Cardiology, vol. 106, pp. 905–912, 2017.
- Virani SS, Alonso A, Benjamin EJ, Bittencourt MS, Callaway CW, Carson AP, Chamberlain AM, Chang AR, Cheng S, Delling FN, Djousse L, Elkind MSV, Ferguson JF, Fornage M, Khan SS, Kissela BM, Knutson KL, Kwan TW, Lackland DT, Lewis TT, Lichtman JH, Longenecker CT, Loop MS, Lutsey PL, Martin SS, Matsushita K, Moran AE, Mussolino ME, Perak AM, Rosamond WD, Roth GA, Sampson UKA, Satou GM, Schroeder EB, Shah SH, Shay CM, Spartano NL, Stokes A, Tirschwell DL, VanWagner LB, Tsao CW, American Heart Association Council on E, Prevention Statistics C, Stroke Statistics S (2020) Heart disease and stroke statistics-2020 update: a report from the American heart association. Circulation, vol. 141, no. 9, pp. e139–e596. https://doi.org/10.1161/CIR.00000000000000757.
- 8. Mao S, Budoff MJ, Bin l, and Liu SC: Optimal ECG trigger point in electron beam CT studies: Three methods for minimizing motion artifacts. Academic Radiology, vol. 8, no. 11, pp. 1107–1115, 2001.
- Husmann L et al.: Coronary artery motion and cardiac phases: Dependency on heart rate—implications for ct image reconstruction. Radiology, vol. 245, no. 2, pp. 567–576, 2007.
- Achenbach S, Delgado V, Hausleiter J, Schoenhagen P, Min JK, Leipsic JA. SCCT expert consensus document on computed tomography imaging before transcatheter aortic valve implantation (TAVI)/transcatheter aortic valve replacement (TAVR). Journal of cardiovascular computed tomography, vol. 6, no. 6, pp. 366–380, 2012.
- Araoz PA, Kirsch J, Primak AN, Braun NN, Saba O, Williamson EE, Harmsen WS, Mandrekar JN, McCollough CH. Optimal image reconstruction phase at low and high heart rates in dualsource CT coronary angiography. The international journal of cardiovascular imaging., vol. 25, pp. 837–845, 2009.



- Zanetti JM, Salerno DM: Seismocardiography: a technique for recording precordial acceleration. Computerbased medical systems. In Proceedings of the Fourth Annual IEEE Symposium on Computer-Based Medical Systems.p. 4-9, 1991.
- 13. Edler I, Lindström K. The history of echocardiography. Ultrasound in medicine & biology;30(12):1565-644, 2004.
- Paukkunen M: Seismocardiography: Practical implementation and feasibility. 2014.
- 15. Yao J, Tridandapani S, Wick CA, and Bhatti PT: Seismocardiography-based cardiac computed tomography gating using patient-specific template identification and detection. IEEE Journal of Translational Engineering in Health and Medicine, vol. 5, pp. 1–14, 2017.
- Di Rienzo M, Vaini E, Castiglioni P, Merati G, Meriggi P, Parati G, Faini A, Rizzo F. Wearable seismocardiography: Towards a beat-by-beat assessment of cardiac mechanics in ambulant subjects. Autonomic Neuroscience, vol. 178, no. 1-2, pp. 50–59, 2013.
- Yao J: Development of a multimodal framework for cardiac computed tomography gating. Ph.D. dissertation, Georgia Institute of Technology, 2018.
- Taebi A, Solar BE, Bomar AJ, Sandler RH, and Mansy HA: Recent advances in seismocardiography. Vibration, vol. 2, no. 1, pp. 64, 2019.
- Yao J, Tridandapani S, Auffermann WF, Wick CA and Bhatti PT: An Adaptive Seismocardiography (SCG)-ECG Multimodal Framework for Cardiac Gating Using Artificial Neural Networks. in IEEE Journal of Translational Engineering in Health and Medicine, vol. 6, pp. 1-11, Art no. 1900611, https://doi.org/10.1109/ JTEHM.2018.2869141, 2018.
- Wick CA, Su JJ, Brand O, McClellan JH, Bhatti PT, Tridandapani S: A trimodal system for the acquisition of synchronous echocardiography, electrocardiography, and seismocardiography data. Annu Int Conf IEEE Eng Med Biol Soc, 6911-4, https://doi.org/ 10.1109/IEMBS.2011.6091740, 2011.
- Wick CA, McClellan JH, Ravichandran L, Tridandapani S: Detection of Cardiac Quiescence from B-Mode Echocardiography Using a Correlation-Based Frame-to-Frame Deviation Measure. IEEE J Transl Eng Health Med. 2013;1:1900211. https://doi.org/10.1109/JTEHM.2013.2291555.
- Walker HK, Hall WD, Hurst JW. Clinical methods: the history, physical, and laboratory examinations, 1990.
- Reinhold J, Rudhe U: Relation of the first and second heart sounds to events in the cardiac cycle. British heart journal 19, no. (4), p. 473, 1957.
- Johansson M: The Hilbert transform, Mathematics Master's Thesis. Växjö University, Suecia. Available online: http://w3.msi.vxu.se/exarb/mj_ex.pdf, consulted on, vol. 19, 1999.

- Wick CA, Inan OT, Bhatti P, Tridandapani S: Relationship between cardiac quiescent periods derived from seismocardiography and echocardiography. In 2015 37th Annual International Conference of the IEEE Engineering in Medicine and Biology Society (EMBC), pp. 687-690, 2015.
- Srichai MB, Hecht EM, Kim D, Babb J, Bod J, Jacobs JE. Dualsource computed tomography angiography image quality in patients with fast heart rates. Journal of cardiovascular computed tomography., 3(5), 300–309. https://doi.org/10.1016/j.jcct.2009.05.014, 2009.
- Yao J, Tridandapani S, Bhatti PT: Near Real-Time Implementation of An Adaptive Seismocardiography - ECG Multimodal Framework for Cardiac Gating. IEEE J Transl Eng Health Med. 2019;7:1900404. https://doi.org/10.1109/JTEHM.2019.2923353, 2019.
- Padmavathi K and Ramakrishna KS: Classification of ECG signal during atrial fibrillation using autoregressive modeling. Procedia Computer Science, vol. 46, pp. 53–59, 2015.
- Taebi A and Mansy HA: Time-frequency distribution of seismocardiographic signals: A comparative study. Bioengineering, vol. 4, no. 2, p. 32, 2017.
- Ferdinando H, Seppälä E, and Myllylä T: Discrete wavelet transforms-based analysis of accelerometer signals for continuous human cardiac monitoring. Applied Sciences, vol. 11, no. 24, p. 12072, 2021.
- 31. Abdi H and Williams LJ: Principal component analysis. Wiley Interdisciplinary Reviews: Computational Statistics, vol. 2, no. 4, pp. 433–459, 2010.
- 32. Xanthopoulos P, Pardalos PM, Trafalis TB, Xanthopoulos P, Pardalos PM, Trafalis TB: Linear discriminant analysis. Robust data mining, pp.27-33, 2013.
- Jais IK, Ismail AR, Nisa SQ: Adam optimization algorithm for wide and deep neural network. Knowl. Eng. Data Sci.. 2, no.(1), pp.41-6, 2019.
- 34. Landis JR and Koch GG: The measurement of observer agreement for categorical data, Biometrics, pp. 159–174, 1977.
- Wick CA, Auffermann WF, Shah AJ, Inan OT, Bhatti PT, Tridan-dapani S: Echocardiography as an indication of continuous-time cardiac quiescence. Phys Med Biol. 2016 Jul 21;61(14):5297-310. https://doi.org/10.1088/0031-9155/61/14/5297.

Publisher's Note Springer Nature remains neutral with regard to jurisdictional claims in published maps and institutional affiliations.

Springer Nature or its licensor (e.g. a society or other partner) holds exclusive rights to this article under a publishing agreement with the author(s) or other rightsholder(s); author self-archiving of the accepted manuscript version of this article is solely governed by the terms of such publishing agreement and applicable law.

